Cyclic gas-phase heterogeneous process in a metal–organic framework involving a nickel nitrosyl complex†

D. Denysenko and D. Volkmer*

The cubic metal–organic framework MFU-4l ($[Zn_5Cl_4(BTDD)_3]$, H_2-BTDD = bis(1*H*-1,2,3-triazolo[4,5-*b*],[4′,5′-*i*])dibenzo[1,4]dioxin) featuring large pore apertures can be modified post-synthetically *via* partial or complete substitution of peripheral metal sites and chloride side-ligands, thus opening a route towards a large variety of functionalized MOFs. In this way, Ni-MFU-4l-nitrite (or Ni-MFU-4l-NO_2) with an analytically determined chemical composition $[Zn_{2.6}Ni_{2.4}(NO_2)_{2.9}Cl_{1.1}(BTDD)_3]$, containing accessible Ni–NO_2 units, was prepared. Ni-MFU-4l-NO_2 undergoes selective heterogeneous gas-phase reduction by carbon monoxide at 350 °C, leading to formation of Ni–NO units at the peripheral sites of the MFU-4l framework (Ni-MFU-4l-NO). The crystallinity and porosity of the MFU-4l framework are completely retained upon this transformation. The so-formed nickel nitrosyl complex, showing high thermal stability, readily reacts with nitrogen monoxide at room temperature, producing Ni–NO_2 units and dinitrogen monoxide (N_2O). Hence, the reaction of Ni-MFU-4l-NO_2 with CO followed by NO represents a cyclic process with an overall stoichiometry $2NO + CO \rightarrow N_2O + CO_2$, in which the Ni-MFU-4l framework serves as a catalyst. It can be considered as a model process for the removal of highly toxic NO and CO gases, which are converted to non-toxic CO_2 and N_2O. Diffuse reflectance infrared Fourier transform spectroscopic studies show that at least 10 cycles can be repeated. The framework's reactivity drops down by *ca.* 50% after 10 cycles, which is most likely due to the accumulation of highly reactive NO_2 and N_2O_4 contaminants. Therefore, further investigations on characterizing reaction intermediates should be done in order to improve the catalyst's performance. Our results confirm the potential of MFU-4l frameworks as selective single-site catalysts for heterogeneous gas-phase transformations and provide a motivation for further studies.

Chair of Solid State and Materials Science, Institute of Physics, University of Augsburg, Universitätsstrasse 1, D-86159 Augsburg, Germany. E-mail: dirk.volkmer@physik.uni-augsburg.de

† Electronic supplementary information (ESI) available: FT-IR, DRIFT and UV-vis-NIR spectra, gas sorption isotherms, XRPD measurements. See DOI: 10.1039/c7fd00034k

Introduction

Metal–organic frameworks (MOFs) represent a rapidly growing and continuously broadening field of research.[1] Apart from classical applications such as heterogeneous catalysis,[2–5] storage of hydrogen[6] or methane,[7] separation processes in gas and liquid phases,[8,9] and capture of carbon dioxide[10] or toxic gases and vapors,[11] MOFs have been recently suggested for a number of different applications such as sensing,[12] photocatalysis,[13] biomedicine,[14] as membrane separation,[15] luminescent,[16] ferroelectric[17] and proton-conducting materials,[18] as well as materials for electronic and optoelectronic devices,[19] non-linear optics[20] and, last but not least, detection of explosives.[21] Despite extensive studies and a large number of reports, catalysis still remains probably the most challenging application field for MOFs. The major part of catalytic transformations has been performed with framework particles suspended in the liquid phase, whereas gas-phase catalytic reactions with MOFs still remain scarce. In most reported gas-phase transformations MOFs were used as a support for active species. For instance, MOF-5, loaded with Cu and ZnO nanoparticles, has been employed as a catalyst for the synthesis of methanol from a $CO/CO_2/H_2$ mixture.[22] A UiO-66 framework, metallated with V(v) ions at the nodes, was shown to perform catalytic gas-phase oxidative dehydrogenation of cyclohexene.[23] A NU-1000 framework, post-synthetically functionalized with bipyridyl moieties and metallated with $NiCl_2$, was applied for gas-phase dimerization of ethylene.[24] However, the structure of active sites and intermediates is often not well-defined in such cases, rendering the rational design of the catalyst a difficult task. Deciphering the basics of a reaction mechanism requires rational design of the catalyst, a task that should be simplified for MOFs when compared to other heterogeneous catalysts, because the catalytically active sites are incorporated into a structurally well-defined framework. One such example is given by Co-MOF-74, which shows catalytic CO oxidation involving coordinatively unsaturated Co(II) sites.[25]

The presence of coordinatively unsaturated accessible metal sites is one of the most important requirements for a catalytically active MOF.[26] Several well-known MOF families contain open metal sites such as $Cu_3(BTC)_2$ (BTC^{3-} = 1,3,5-benzenetricarboxylate),[27] CPO-27 (ref. 28) or MOF-74,[29] and $Mn_3[(MnCl)_4(BTT)_8]_2$ (H_3-BTT = benzene-1,3,5-tris(1*H*-tetrazole)).[30] In recent years our group has developed a family of MFU-4-type frameworks comprising coordinatively unsaturated metal sites. While the parent compound, MFU-4, has very narrow pore apertures and, therefore, is not suitable for catalytic applications,[31] its large-pore analogue MFU-4l ($[Zn_5Cl_4(BTDD)_3]$, H_2-BTDD = bis(1*H*-1,2,3-triazolo[4,5-*b*],[4′,5′-*i*])dibenzo[1,4]dioxin) provides an opportunity for catalytic transformations.[32] The secondary building unit (SBU) of MFU-4l consists of a single octahedrally and four tetrahedrally coordinated Zn ions which are interconnected by six triazolate ligands, building a so-called Kuratowski unit.[33] Each tetrahedral (peripheral) zinc ion in addition becomes coordinated by a chloride side-ligand, leading to a coordination environment which is very similar to the well-known scorpionate complexes.[34]

Such construction of the SBU allows us to obtain a large variety of substituted MFU-4l frameworks *via* post-synthetic metal- and side-ligand exchange reactions (Scheme 1a). Previously we have described Mn(II), Fe(II), Co(II), Ni(II), Cu(II), Cu(I)

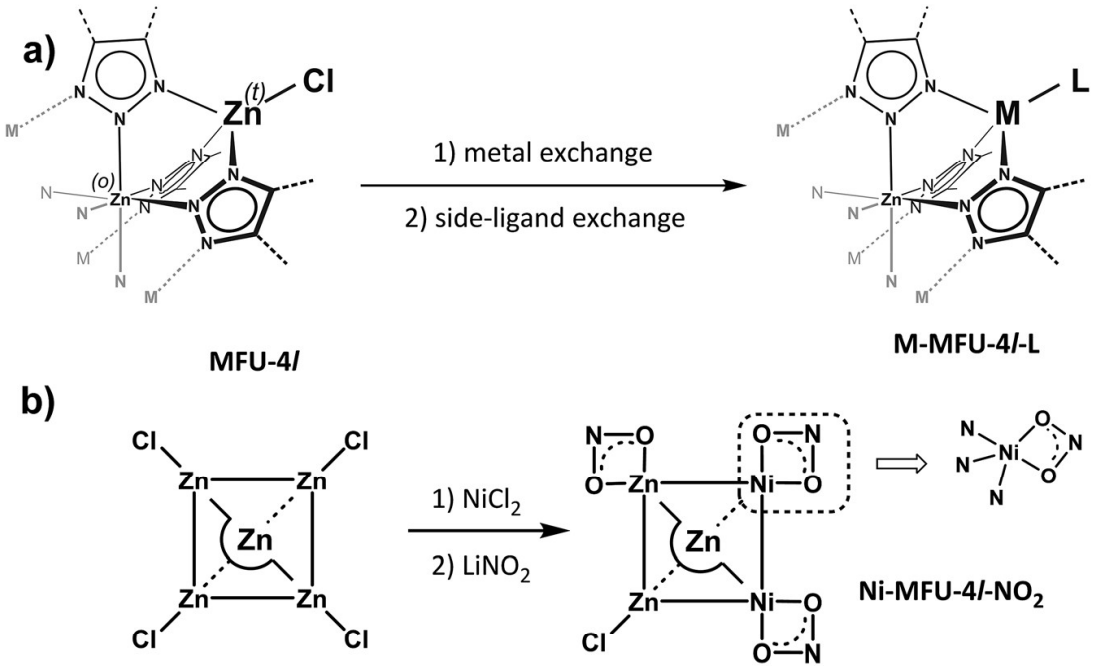

Scheme 1 (a) Post-synthetic metal- and side-ligand exchange reactions in MFU-4l at peripheral sites (a part of the SBU is shown, t – tetrahedral, o – octahedral), (b) schematic representation of the Kuratowski unit in MFU-4l and synthesis of MFU-4l-NO_2 (an idealized composition is shown, in the following schemes only one peripheral Ni-center is shown).

and Li-derivatives of MFU-4l with different mono- and bidentate side-ligands.[35–38] In the case of Co(II) all four peripheral Zn–Cl units can substituted, in other cases only partial substitution has been achieved. In no case investigated so far has the central octahedrally coordinated Zn ion been post-synthetically exchanged against other metal ions. The group of Dincă subsequently has extended the MFU-4l family with Ti(III), Ti(IV), Cr(II) and Cr(III) derivatives.[39] The possibility of introducing almost any desired metal ion, as well as the free accessibility of the peripheral metal sites, makes MFU-4l a perfect framework for designing heterogeneous catalysts. We have previously shown that Cu(I) sites in MFU-4l are highly active and bind H_2, D_2, N_2, or O_2 molecules stoichiometrically with isosteric heats of adsorption of 32, 35, 42 and 53 kJ mol^{-1}, respectively.[36,40] Ni-MFU-4l was found to be a highly efficient catalyst for selective ethylene dimerization in toluene with either methylaluminoxane (MAO) or modified methylaluminoxane (MMAO-12) serving as an activating agent.[41,42] We could show that peripheral metal sites in MFU-4l can serve as single-site active centers in heterogeneous gas-phase transformations. Thus, Cu(II)–F units are converted to Cu(I) *via* a Cu(II)–H intermediate upon reaction with hydrogen under mild conditions (240 °C, 100 mbar H_2 partial pressure).[37] Co-MFU-4l, on the other hand, was shown to perform multiple and reversible gas-phase oxidation by O_2 followed by reduction by CO.[35] However, the reaction mechanism in this case is not fully clear and the catalytic activity might also be related to active cobalt sites caused by framework defects. Herein we report on the first gas-phase multiple-step cyclic heterogeneous process in a MFU-4l framework involving a nickel nitrosyl complex. This sequence serves as a "proof of principle" and confirms the potential of MFU-4l frameworks for the development of selective catalysts with single-site active centers.

Experimental

Materials and methods

All starting materials were of reagent grade and used as received from the commercial supplier. Fourier transform infrared (FTIR) spectra were recorded with an ATR unit in the range 4000–400 cm^{-1} on a Bruker Equinox 55 FT-IR spectrometer. The following indicators are used to characterize absorption bands: very strong (vs), strong (s), medium (m), weak (w), shoulder (sh). Diffuse reflectance infrared Fourier transform (DRIFT) spectra were recorded with the same instrument equipped with a Harrick Praying Mantis reaction chamber. The sample was grinded with KBr (at approx. 0.01 wt% concentration), and pure KBr was used as a reference. Diffuse reflectance UV-vis-NIR spectra were recorded in the 2000–250 nm range on a Perkin Elmer λ 750s spectrometer equipped with a Labsphere 60 mm RSA ASSY integrating sphere with a 0°/d measuring geometry. Labsphere Spectralon SRS-99 was used as the white standard. *In situ* UV-vis-NIR spectra were recorded with the same instrument equipped with a Harrick Praying Mantis reaction chamber. High-purity barium sulfate (99.998%, Aldrich) was used as the white standard. High-purity nitrogen monoxide (>99.999%, 5% in Ar) gas was used for *in situ* spectroscopic measurements. Thermogravimetric analysis (TGA) under N_2 and H_2 (10% in Ar) gas flow was performed with a TA Instruments Q500 analyzer at a heating rate of 5 K min^{-1}. TGA under CO (10% in Ar) gas flow was performed with a Netzsch STA 409 PC Luxx instrument at the heating rate of 5 K min^{-1}. Preparative thermolysis under CO (10% in Ar) gas flow was performed in the Nabertherm P330 tube furnace using an aluminium oxide crucible and a borosilicate glass tube. Energy-dispersive X-ray spectroscopy (EDX) was performed with a Philips XL 30 FEG scanning electron microscope equipped with an EDAX SiLi detector. An area of at least 10 × 10 μm including at least 10 MOF crystals was scanned. N_2 adsorption isotherms for the determination of BET surface areas were measured at 77 K in the relative pressure range 0.01–0.45 with a Quantachrome NOVA 2000 Series instrument. Adsorbed amounts are given in cm^3 g^{-1} [STP], where STP = 100 kPa and 273.15 K. Prior to measurements, the samples were degassed at 100 °C for 3 h under vacuum. Powder X-ray diffraction data were collected in the 2θ range of 4–40° with 0.02° steps, with a time of 1 s per step, using a Seifert XRD 3003 TT diffractometer equipped with a Meteor 1D detector.

Preparation of Ni-MFU-4l-NO_2

Ni-MFU-4l was prepared as described previously.[37] The side-ligand exchange was performed similarly to a previously published procedure:[37] a 1 M solution of $LiNO_2$ in methanol (0.4 mL, 0.4 mmol) was added to a suspension of Ni-MFU-4l (150 mg, approx. 0.12 mmol) in acetonitrile (30 mL) and the mixture was stirred for 30 min at room temperature. The precipitate was filtered off, washed with methanol and CH_2Cl_2 and dried at 80 °C under vacuum, yielding 140 mg of a greenish-yellow product. Zn/Ni/Cl ratio: 2.60/2.40/1.14, framework composition: $Zn_{2.6}Ni_{2.4}(NO_2)_{2.9}Cl_{1.1}(BTDD)_3$. IR (ATR, cm^{-1}): 1625 (w), 1575 (w), 1461 (vs), 1351 (vs), 1210 (sh), 1183 (vs), 1061 (w), 922 (s), 867 (m), 817 (m), 535 (m), 429 (w). BET surface area (N_2, 77.3 K): 3332 m^2 g^{-1}.

Preparation of Ni-MFU-4l-NO

Ni-MFU-4l-nitrite (100 mg, approx. 0.08 mmol) was heated in a tube furnace under a 70 mL min^{-1} flow of CO (10% in Ar) with a rate of 3 K min^{-1} up to 375 °C, holding the sample at the final temperature for 30 min followed by cooling down to room temperature. 90 mg of a deep-blue coloured product was obtained. IR (ATR, cm^{-1}): 3080 (w), 1809 (m), 1625 (w), 1577 (w), 1461 (vs), 1351 (vs), 1184 (vs), 1055 (w), 918 (s), 868 (m), 849 (m), 816 (w), 535 (m), 427 (w). BET surface area (N_2, 77.3 K): 3746 m^2 g^{-1}.

Results

Preparation and characterization of Ni-MFU-4l-NO

Ni-MFU-4l-nitrite was prepared by a side-ligand substitution reaction similarly to a previously described procedure.[37] The Zn/Ni/Cl ratio, calculated from EDX data, shows that on average two out of four peripheral zinc ions have been substituted by nickel and three out of four chloride side-ligands have been substituted by nitrite. Based on our previous studies showing that side-ligand exchange proceeds more readily at 3d transition metal centers,[37] we assume that the remaining chloride is preferably coordinated to zinc ions (as shown in Scheme 1b). The TGA curve of Ni-MFU-4l-NO_2 under nitrogen shows a small weight-loss step between 275 and 375 °C, which should be related to the decomposition of nitrite side-ligands (Fig. 1, green curve). When the experiment is performed under a carbon monoxide (10% in Ar) gas flow, the weight loss starts readily at lower temperature and is finished at *ca.* 340 °C, where a stable plateau is reached (Fig. 1, red curve). The obtained deep-blue coloured product retains a highly crystalline MFU-4l framework structure, as shown by the corresponding XRPD pattern (*cf.* ESI, Fig. S9†). Intactness of the MFU-4l structure is also confirmed by the nitrogen adsorption isotherm sampled at 77 K, revealing a high BET surface area of 3746 m^2 g^{-1} which is typical for MFU-4l-type frameworks (*cf.* ESI, Fig. S10†). The IR spectrum of this product shows a characteristic band at 1809 cm^{-1} (*cf.* ESI, Fig. S2†), which allows us to identify it as nickel nitrosyl complex (Scheme 2). This band corresponds to the N–O stretching frequency and is very similar to that

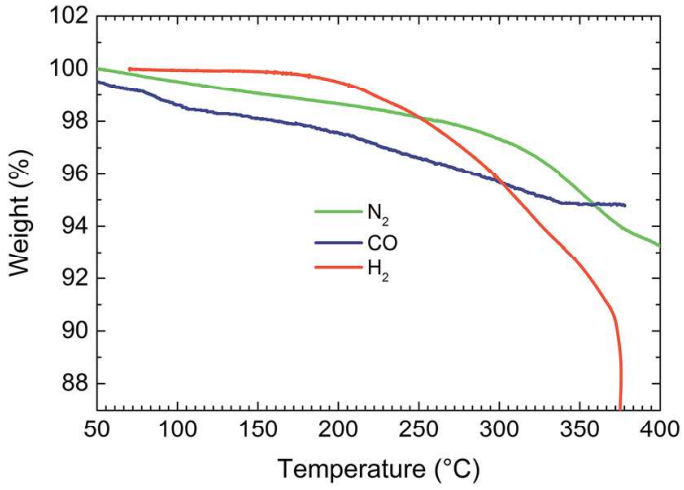

Fig. 1 TGA curves for Ni-MFU-4l-NO_2 under N_2 (green), 10% CO in Ar (blue) and 10% H_2 in Ar (red) gas flow.

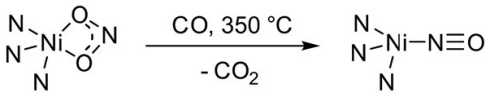

Scheme 2 Formation of Ni-MFU-4l-NO from Ni-MFU-4l-NO_2 upon reaction with 10% CO in Ar at 350 °C.

determined for a scorpionate nickel nitrosyl complex [(Tp^{Me_2})Ni(NO)] (1786 cm^{-1}, Tp^{Me_2} = hydrotris(3-isopropyl-5-methyl-1-pyrazolyl)borate).[43] A frequency shift to higher values hints at lower Ni → NO (π*) back donation and thus speaks in favour of weaker electron-donating properties of the triazolate ligands as compared to a pyrazolate-based scorpionate.

It should be noted that the reaction of Ni-MFU-4l-NO_2 with hydrogen also leads to a Ni–nitrosyl complex (as confirmed by IR spectroscopy), but no stable plateau can be seen in the TGA curve (Fig. 1, red curve). According to this finding, the reaction is accompanied by the partial decomposition of the framework and thus is not suitable for the preparation of Ni-MFU-4l-NO.

Noticeably, Co-MFU-4l-nitrite doesn't form a nitrosyl complex upon reaction with carbon monoxide at 350 °C, but reacts to isocyanate (Scheme 3), as can be seen by a characteristic IR band at 2217 cm^{-1} with a shoulder, which is also present in Co-MFU-4l-isocyanate, prepared *via* post-synthetic side-ligand exchange (*cf.* ESI, Fig. S3†).[37]

The UV-vis-NIR spectrum of Ni-MFU-4l-NO shows a very intensive absorption band with λ_{max} = 610 nm, responsible for the deep-blue colour of this compound (Fig. 2, full UV range is shown in ESI, Fig. S5†). A similar absorption band with λ_{max} = 630 nm was also found in a scorpionate complex [($Tp^{t\text{-}Bu,i\text{-}Pr}$)Ni(NO)] ($Tp^{t\text{-}Bu,i\text{-}Pr}$ = hydrotris(3-*tert*-butyl-5-isopropyl-1-pyrazolyl)borate).[44] This band most likely corresponds to a spin-allowed $^3T_1(F) \rightarrow {}^3T_1(P)$ d–d transition of tetrahedrally coordinated high-spin Ni(II) and therefore speaks for the nickel oxidation state of +II and the NO ligand present as NO^- in a nickel nitrosyl complex. This assumption was confirmed by multi-edge XAS measurements and DFT calculations.[44] The UV-vis-NIR spectrum of greenish-yellow Ni-MFU-4l-NO_2 (Fig. 2 and ESI, Fig. S6†) shows only weak absorption bands with λ_{max} = 687, 805, 890 and 1439 nm, which point to five-fold coordinated Ni^{2+} ions rather than tetrahedrally coordinated metal species. The latter ones, by analogy to tetrahedrally coordinated Co^{2+}, should show a stronger absorption band at *ca.* 600 nm leading to a blue colour.[45] Thus, the nitrite side-ligand in Ni-MFU-4l-NO_2 is most likely coordinated *via* its oxygen atoms in a bidentate fashion, assuming that the mechanism of the reaction with CO might first include the isomerization of bidentate nitrite (Ni–ONO) to a monodentate N-coordinated one (Ni–NO_2), before the Ni–NO complex is formed.

Interestingly, Mistry and Natarajan have reported the dark-blue coloured nickel carbonyl complexes $[Ni_5(bta)_6(CO)_4]$, $[Ni_9(bta)_{12}(CO)_6]$, and

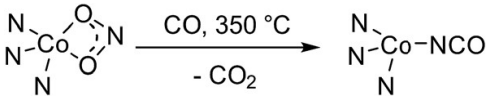

Scheme 3 Formation of Co-MFU-4l-NCO from Co-MFU-4l-NO_2 upon reaction with 10% CO in Ar at 350 °C.

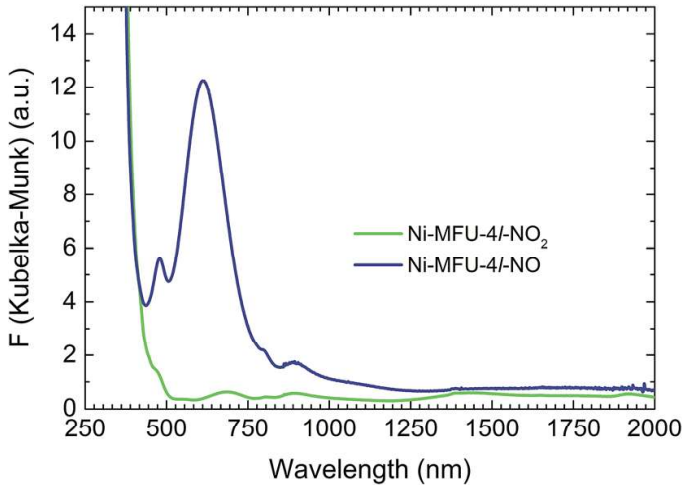

Fig. 2 UV-vis-NIR spectra of Ni-MFU-4l-NO_2 (green) and Ni-MFU-4l-NO (blue).

$[Ni_9(bta)_{12}(CO)_6]\cdot 2DMF$, obtained upon heating nickel nitrate hexahydrate with benzotriazole (H-bta) in *N*,*N*-dimethylformamide (DMF) at 150–180 °C.[46] However, their structural and chemical characterization seems to be questionable, since an intense blue colour should rather speak for a nickel nitrosyl and not a carbonyl complex. Moreover, the reported "$[Ni_9(bta)_{12}(CO)_6]$" complex shows an IR absorption band at 1789 cm^{-1} which should rather correspond to a Ni–NO complex and not to Ni–CO, as indicated by the fact that the C–O valence stretching frequency is usually found at approx. 2000 cm^{-1} (2022 cm^{-1} for $[L^{Me}Ni(CO)]$, L^{Me} = *N*,*N*′-bis(2,6-diisopropylphenyl)-β-diketiminate[47] and 1999 cm^{-1} for $[(PhTt^{t\text{-}Bu})Ni(CO)]$, $PhTt^{t\text{-}Bu}$ = phenyltris((*tert*-butylthio)methyl)borate[48]). Also the reported very short "Ni–C" bond distances of 1.62–1.64 Å rather match the Ni–N distance in nitrosyl complexes (1.62 Å for $[(Tp^{Me_2})Ni(NO)]$[43]), whereas typical Ni–C bond distances in carbonyl complexes are found to be larger (1.77 Å for $[L^{Me}Ni(CO)]$[47] and 1.75 Å for $[(PhTt^{t\text{-}Bu})Ni(CO)]$[48]).

Reaction of Ni-MFU-4l-NO with nitrogen monoxide and cyclic reactivity studies

Ni-MFU-4l-NO readily reacts with NO at room temperature producing Ni-MFU-4l-nitrite, which allows the running of a cyclic process. Formation of initial nickel nitrite species is confirmed by *in situ* UV-vis-NIR measurements (*cf.* ESI, Fig. S7 and S8†). In this experiment, Ni-MFU-4l-NO was first dried in an argon flow at 150 °C and then cooled down to room temperature, before the gas was switched to 5% NO in Ar. After 20 min, the gas flow was switched back to Ar and the DRIFT spectrum was recorded, revealing the same absorption bands as a reference sample of Ni-MFU-4l-NO_2 measured in the integrating sphere. The putative mechanism of such a reaction was studied previously for a $[Ni(NO)(bipy)(Me_2\text{-}phen)]^+[PF_6]^-$ complex in dichloromethane solution (bipy = 2,2′-bipyridyl, Me_2-phen = 2,9-dimethyl-1,10-phenanthroline).[49] It was shown that the reaction proceeds *via* a *cis*-hyponitrite ($N_2O_2^{2-}$) intermediate and results in NO disproportionation to NO_2^- and N_2O, as shown in Scheme 4. A similar *cis*-hyponitrite complex $[Ni(k^2\text{-}O_2N_2)(bipy)]$, obtained *via* coordinative disproportionation of $[Ni(NO)(bipy)_2]^+[PF_6]^-$, was isolated and characterized by the same research group previously.[50]

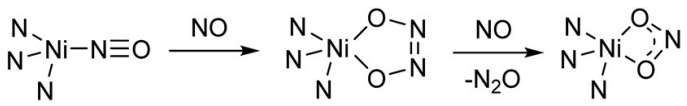

Scheme 4 Schematic representation of the reaction of a nickel nitrosyl coordination unit with NO, including a *cis*-hyponitrite reaction intermediate.

In order to study the repeatability of this cyclic process, we have conducted *in situ* DRIFT studies. First, Ni-MFU-4l-NO_2 was converted to Ni-MFU-4l-NO upon heating under 10% CO in an Ar gas flow up to 350 °C and holding the sample for 10 min at this temperature. Then the gas flow was switched to nitrogen and the sample was allowed to cool down to 40 °C. At this point the spectrum was measured and then the gas was switched to 5% NO in Ar. After 5 min, the gas was switched back to nitrogen, upon which the sample was flushed for another 10 min and the spectrum was recorded. After this the gas was switched to 10% CO in Ar and the sequence was repeated. Altogether we have conducted 10 reaction cycles. IR spectra show reversible formation of a nickel nitrosyl complex, as indicated by the appearance and loss of the band at 1809 cm^{-1} (Fig. 3, for complete data see ESI, Fig. S4†). However, the intensity of this band decreases stepwise, reaching a final value of approx. 50% (as compared to the initial intensity) after 10 cycles. At the same time, a number of new bands centered at 3441, 3355, 2763, 2425, 2170, 2092, 1767, 1439, 1333, 1269 and 839 cm^{-1} start to appear (marked with asterisks in Fig. 3 and ESI, Fig. S4†). As some of these bands at 2763, 2425, 1767, 1439, 1333 and 839 cm^{-1} can also be observed in a control experiment with a microporous metal-free carbon reference compound, they can be assigned to accumulating nitrogen oxide (NO_2 and N_2O_4) species. Other bands at 3441, 3355, 2170, 2092 and 1269 cm^{-1} could be most likely assigned to reaction products between NO_2/N_2O_4 and the MFU-4l framework. Unfortunately, up to now we couldn't manage to avoid accumulation of NO_2/N_2O_4 impurities despite using high-purity (>99.999%)

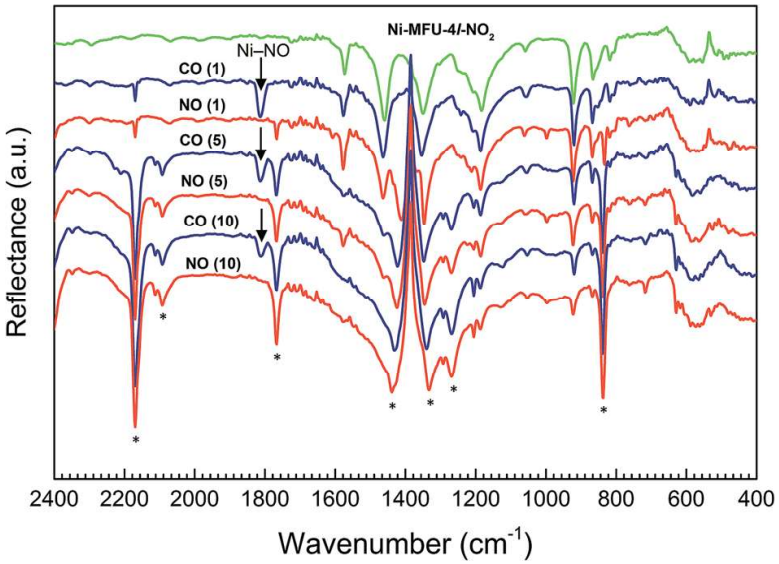

Fig. 3 DRIFT spectra of Ni-MFU-4l-NO_2 (green) after treatment with CO (blue) at 350 °C and subsequent treatment with NO (red) at 40 °C (gas type and cycle number are marked on top of the corresponding spectrum); bands marked with an asterisk indicate side products due to accumulation of NO_2 and N_2O_4 impurities.

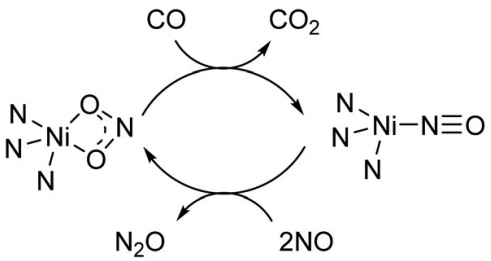

Scheme 5 Cyclic conversion of Ni-MFU-4l-NO_2 to Ni-MFU-4l-NO and back upon reaction with CO and NO, respectively.

gases. Since a very low amount of a MOF (*ca.* 0.1 mg) is used in DRIFT experiments, trace impurities are sufficient to observe such side effects. Nevertheless we assume that the observed decrease of the intensity of the N–O vibrational band and the corresponding framework degradation is caused by highly reactive NO_2/N_2O_4 contaminants and is not due to the cyclic reaction sequence employing CO/NO. In order to prove this, additional experiments with even more pure gases or a larger amount of a MOF will be required.

Combining both reactions, the cycle leads to a net equation $2NO + CO \rightarrow N_2O + CO_2$, in which the Ni-MFU-4l framework serves as a catalyst (Scheme 5). Hence, this sequence can be seen as a catalytic conversion of highly toxic CO and NO gases into non-toxic CO_2 and N_2O.

Previously it was shown that a Fe-MOF-5 framework performs a disproportionation of nitrogen monoxide to nitrous oxide and nitrite.[51] In this case, NO first binds to a Fe(II) center, forming a nitrosyl complex which then reacts with another two equivalents of NO to form N_2O and NO_2^-, bound to the Fe(III) center. Mechanistic studies have shown that this reaction also proceeds *via* the hyponitrite intermediate. It should be noted that the authors in these studies focused on a non-cyclic process and further investigations targeting on the possibility to convert Fe(III)–NO_2 units back to Fe(III)–NO might be interesting.

Conclusions

We have shown that Ni-MFU-4l-nitrite selectively reacts with carbon monoxide at 350 °C producing a nickel nitrosyl complex at the peripheral sites of the MFU-4l framework. To the best of our knowledge, this is the first example demonstrating the formation of a Ni–NO complex *via* heterogeneous gas-phase reduction of Ni-nitrite moieties. This nickel nitrosyl complex readily reacts with nitrogen monoxide at room temperature, restoring Ni-MFU-4l-nitrite and nitrous oxide (N_2O). Hence, the overall conversion in this cycle is described by the net equation $2NO + CO \rightarrow N_2O + CO_2$, in which the Ni-MFU-4l framework serves as a catalyst. This conversion, taking place at single-site active centers in the MFU-4l framework, can be regarded as a model process for the removal of highly toxic NO and CO gases, by converting them into non-toxic CO_2 and N_2O.

Repeatability studies, monitored by *in situ* DRIFT spectroscopy, have shown that at least 10 reaction cycles can be repeated. However, degradation of the framework accompanied by the appearance of several additional peaks, being assigned to the presence of NO_2 and N_2O_4 contaminants, is also observed. This points to the problem of limited stability of the MFU-4l framework in the presence

of such highly reactive nitrogen oxides. We assume that nitrogen monoxide would not cause the decay of the MFU-4l framework, so that the cyclic exposure performed with ultra-pure NO gas (under rigorous exclusion of moisture and air) should be repeatable without significant loss of the reactivity of the MOF. In order to prove this, additional experiments with an improved gas and experimental setup will be necessary.

The results presented in this study add further impetus to the previously demonstrated potential of MFU-4l frameworks being employed as selective single-site catalysts for heterogeneous gas-phase transformations. Further studies in order to optimize the process and characterize intermediates should be highly rewarding. Also the use of chemically more stable frameworks (containing fluorinated linkers, for instance) should be considered for this application.

Acknowledgements

D. D. gratefully acknowledges financial support from the University of Augsburg.

References

1 H.-C. J. Zhou and S. Kitagawa, *Chem. Soc. Rev.*, 2014, **43**, 5415–5418.
2 J. Gascon, A. Korma, F. Kapteijn and F. X. Llabrés i. Xamena, *ACS Catal.*, 2014, **4**, 361–378.
3 J. Liu, L. Chen, H. Cui, J. Zhang, L. Zhang and C.-Y. Su, *Chem. Soc. Rev.*, 2014, **43**, 6011–6061.
4 K. Leus, Y.-Y. Liu and P. Van Der Voort, *Catal. Rev. Sci. Eng.*, 2014, **56**, 1–56.
5 P. García-García, M. Müller and A. Corma, *Chem. Sci.*, 2014, **5**, 2979–3007.
6 M. P. Suh, H. J. Park, T. K. Prasad and D.-W. Lim, *Chem. Rev.*, 2012, **112**, 782–835.
7 Y. He, W. Zhou, G. Qian and B. Chen, *Chem. Soc. Rev.*, 2014, **43**, 5657–5678.
8 J.-R. Li, J. Sculley and H.-C. Zhou, *Chem. Rev.*, 2012, **112**, 869–932.
9 B. Van de Voorde, B. Bueken, J. Denayer and D. De Vos, *Chem. Soc. Rev.*, 2014, **43**, 5766–5788.
10 K. Sumida, D. L. Rogow, J. A. Mason, T. M. McDonald, E. D. Bloch, Z. R. Herm, T.-H. Bae and J. R. Long, *Chem. Rev.*, 2012, **112**, 724–781.
11 E. Barea, C. Montoro and J. A. R. Navarro, *Chem. Soc. Rev.*, 2014, **43**, 5419–5430.
12 L. E. Kreno, K. Leong, O. K. Farha, M. Allendorf, R. P. Van Duyne and J. T. Hupp, *Chem. Rev.*, 2012, **112**, 1105–1125.
13 T. Zhang and W. Lin, *Chem. Soc. Rev.*, 2014, **43**, 5982–5993.
14 P. Horcajada, R. Gref, T. Baati, P. K. Allan, G. Maurin, P. Couvreur, G. Férey, R. E. Morris and C. Serre, *Chem. Rev.*, 2012, **112**, 1232–1268.
15 S. Qiu, M. Xue and G. Zhu, *Chem. Soc. Rev.*, 2014, **43**, 6116–6140.
16 Y. Cui, Y. Yue, G. Qian and B. Chen, *Chem. Rev.*, 2012, **112**, 1126–1162.
17 W. Zhang and R.-G. Xiong, *Chem. Rev.*, 2012, **112**, 1163–1195.
18 P. Ramaswamy, N. E. Wong and G. K. H. Shimizu, *Chem. Soc. Rev.*, 2014, **43**, 5913–5932.
19 V. Stavila, A. A. Talin and M. D. Allendorf, *Chem. Soc. Rev.*, 2014, **43**, 5994–6010.
20 C. Wang, T. Zhang and W. Lin, *Chem. Rev.*, 2012, **112**, 1084–1104.
21 Z. Hu, B. J. Deibert and J. Li, *Chem. Soc. Rev.*, 2014, **43**, 5815–5840.

22 M. Müller, S. Hermes, K. Kähler, M. W. E. van der Berg, M. Muhler and R. A. Fischer, *Chem. Mater.*, 2008, **20**, 4576–4587.
23 H. G. T. Nguyen, N. M. Schweitzer, C.-Y. Chang, T. L. Drake, M. C. So, P. C. Stair, O. K. Farha, J. T. Hupp and S. T. Nguyen, *ACS Catal.*, 2014, **4**, 2496–2500.
24 S. T. Madrahimov, J. R. Gallacher, G. Zhang, Z. Meinhart, S. J. Garibay, M. Delferro, J. T. Miller, O. K. Farha, J. T. Hupp and S. T. Nguyen, *ACS Catal.*, 2015, **5**, 6713–6718.
25 T. Kim, D. H. Kim, S. Kim, Y. D. Kim, Y.-S. Bae and C. Y. Lee, *Polyhedron*, 2015, **90**, 18–22.
26 P. Valvekens, F. Vermoortele and D. De Vos, *Catal. Sci. Technol.*, 2013, **3**, 1435–1445.
27 S. S.-Y. Chui, S. M.-F. Lo, J. P. H. Charmant, A. G. Orpen and I. D. Williams, *Science*, 1999, **283**, 1148–1150.
28 P. D. C. Dietzel, Y. Morita, R. Blom and H. Fjellvåg, *Angew. Chem., Int. Ed.*, 2005, **44**, 6354–6358.
29 N. L. Rosi, J. Kim, M. Eddaoudi, B. Chen, M. O'Keeffe and O. M. Yaghi, *J. Am. Chem. Soc.*, 2005, **127**, 1504–1518.
30 M. Dincă, A. Dailly, Y. Liu, C. M. Brown, D. A. Neumann and J. R. Long, *J. Am. Chem. Soc.*, 2006, **128**, 16876–16883.
31 S. Biswas, M. Grzywa, H. P. Nayek, S. Dehnen, I. Senkovska, S. Kaskel and D. Volkmer, *Dalton Trans.*, 2009, 6487–6495.
32 D. Denysenko, M. Grzywa, M. Tonigold, B. Streppel, I. Krkljus, M. Hirscher, E. Mugnaioli, U. Kolb, J. Hanss and D. Volkmer, *Chem.–Eur. J.*, 2011, **17**, 1837–1848.
33 S. Biswas, M. Tonigold, M. Speldrich, P. Kögerler, M. Weil and D. Volkmer, *Inorg. Chem.*, 2010, **49**, 7424–7434.
34 S. Trofimenko, *Chem. Rev.*, 1993, **93**, 943–980.
35 D. Denysenko, T. Werner, M. Grzywa, A. Puls, V. Hagen, G. Eickerling, J. Jelic, K. Reuter and D. Volkmer, *Chem. Commun.*, 2012, **48**, 1236–1238.
36 D. Denysenko, M. Grzywa, J. Jelic, K. Reuter and D. Volkmer, *Angew. Chem., Int. Ed.*, 2014, **53**, 5832–5836.
37 D. Denysenko, J. Jelic, K. Reuter and D. Volkmer, *Chem.–Eur. J.*, 2015, **21**, 8188–8199.
38 D. Denysenko, J. Jelic, O. V. Magdysyuk, K. Reuter and D. Volkmer, *Microporous Mesoporous Mater.*, 2015, **216**, 146–150.
39 R. J. Comito, K. J. Fritzsching, B. J. Sundell, K. Schmidt-Rohr and M. Dincă, *J. Am. Chem. Soc.*, 2016, **138**, 10232–10237.
40 I. Weinrauch, I. Savchenko, D. Denysenko, S. M. Souliou, H.-H. Kim, M. Le Tacon, L. L. Daemen, Y. Cheng, A. Mavrandonakis, A. J. Ramirez-Cuesta, D. Volkmer, G. Schütz, M. Hirscher and T. Heine, *Nat. Commun.*, 2017, **8**, 14496.
41 E. D. Metzger, C. K. Brozek, R. J. Comito and M. Dincă, *ACS Cent. Sci.*, 2016, **2**, 148–153.
42 E. D. Metzger, R. J. Comito, C. H. Hendon and M. Dincă, *J. Am. Chem. Soc.*, 2017, **139**, 757–762.
43 E. D. Metzger, C. K. Brozek, R. J. Comito and M. Dincă, *Dalton Trans.*, 2007, **2**, 820–824.

44 S. Soma, C. Van Stappen, M. Kiss, R. K. Szilagyi, N. Lehnert and K. Fujisawa, *JBIC, J. Biol. Inorg. Chem.*, 2016, **21**, 757–775.
45 A. B. P. Lever, in *Inorganic electronic spectroscopy*, Elsevier, Amsterdam, 2nd edn, 1984, pp. 507–544.
46 S. Mistry and S. Natarajan, *J. Chem. Sci.*, 2014, **126**, 1477–1491.
47 N. A. Eckert, A. Dinescu, T. R. Cundari and P. L. Holland, *Inorg. Chem.*, 2005, **44**, 7702–7704.
48 P. J. Schebler, B. S. Mandimutsira, C. G. Riordan, L. M. Liable-Sands, C. D. Incarvito and A. L. Rheingold, *J. Am. Chem. Soc.*, 2001, **123**, 331–332.
49 A. M. Wright, H. T. Zaman, G. Wu and T. W. Hayton, *Inorg. Chem.*, 2014, **53**, 3108–3116.
50 A. M. Wright, G. Wu and T. W. Hayton, *J. Am. Chem. Soc.*, 2012, **134**, 9930–9933.
51 C. K. Brozek, J. T. Miller, S. A. Stoian and M. Dincă, *J. Am. Chem. Soc.*, 2015, **137**, 7495–7501.